AIP Advances

Comparison of the electronic and thermoelectric properties of three layered phases Bi_2Te_3, $PbBi_2Te_4$ and $PbBi_4Te_7$: LEGO thermoelectrics

Cite as: AIP Advances **8**, 115213 (2018); https://doi.org/10.1063/1.5047823
Submitted: 10 July 2018 . Accepted: 05 November 2018 . Published Online: 14 November 2018

Changhoon Lee, Jae Nyeong Kim, Jang-Yeul Tak, Hyung Koun Cho, Ji Hoon Shim, Young Soo Lim, and Myung-Hwan Whangbo

Comparison of the electronic and thermoelectric properties of three layered phases Bi_2Te_3, $PbBi_2Te_4$ and $PbBi_4Te_7$: LEGO thermoelectrics

Changhoon Lee,[1,2] Jae Nyeong Kim,[1,a] Jang-Yeul Tak,[3] Hyung Koun Cho,[3] Ji Hoon Shim,[1,2,b] Young Soo Lim,[4,b] and Myung-Hwan Whangbo[5,b]
[1]*Department of Chemistry, Pohang University of Science and Technology, Pohang 37673, Korea*
[2]*Division of Advanced Nuclear Engineering, Pohang University of Science and Technology, Pohang 37673, Korea*
[3]*School of Advanced Materials Science and Engineering, Sungkyunkwan University, Suwon 16419, Korea*
[4]*Department of Materials System Engineering, Pukyong National University, Busan 48547, Korea*
[5]*Department of Chemistry, North Carolina State University, Raleigh, North Carolina 27695-8204, USA*

(Received 10 July 2018; accepted 5 November 2018; published online 14 November 2018)

The electronic and thermoelectric properties of Bi_2Te_3, $PbBi_2Te_4$ and $PbBi_4Te_7$ were examined on the basis of density functional theory (DFT) calculations and thermoelectric transport property measurements. The layered phase $PbBi_4Te_7$ is composed of the slabs forming the layered phases Bi_2Te_3 and $PbBi_2Te_4$. The electronic structure of $PbBi_4Te_7$ around the valence band maximum and conduction band minimum exhibits those of Bi_2Te_3 and $PbBi_2Te_4$. The band gap of $PbBi_4Te_7$ lies in between those of Bi_2Te_3 and $PbBi_2Te_4$, and the density of states of $PbBi_4Te_7$ is well approximated by the sum of those of Bi_2Te_3 and $PbBi_2Te_4$. In terms of the carrier concentration, the carrier mobility, the carrier lifetime, the electrical conductivity normalized to the carrier lifetime, and the effective mass, the layered phases Bi_2Te_3, $PbBi_4Te_7$ and $PbBi_2Te_4$ form a group of thermoelectrics, which have the structures composed of several different slabs and whose thermoelectric properties are approximated by the average of those of the constituent slabs. We propose to use the term "LEGO thermoelectrics" to describe such a family of thermoelectric materials that operate in a desired temperature range and possess predictable thermoelectric properties.
https://doi.org/10.1063/1.5047823

I. INTRODUCTION

Over the past several decades, thermoelectric materials have been extensively studied because of their ability to convert heat into electricity and their potential use in generating primary power and recovering waste heat.[1–3] Since their discovery in the 1950s, Bi_2Te_3 and PbTe are still the best thermoelectric materials around room temperature and in the medium temperature range, respectively, and have been widely used in thermoelectric modules.[4–6] It has been a challenging task to find more efficient thermoelectric materials. At a given temperature T, the efficiency of a thermoelectric material is measured by its figure of merit ZT, a dimensionless quantity,

[a]Present address: DRAM Product & Technology, Memory Business, Samsung Electronics, 1 Samsungjeonja-ro, Hwasung-si, Gyeonggi-do, 18448, Korea.
[b]Corresponding author: jhshim@postech.ac.kr, yslim@pknu.ac.kr, whangbo@ncsu.edu

$$ZT = \frac{S^2\sigma}{\kappa}T, \quad (1)$$

where S is the Seebeck coefficient, σ the electrical conductivity, and κ the thermal conductivity.[7] Efforts made to improve the thermoelectric properties on Bi_2Te_3 and PbTe systems can be grouped into either enhancing the power factor $S^2\sigma$[8–18] (e.g., optimizing the carrier density, band engineering, using quantum confinement effects, and electron energy filtering) or reducing the lattice thermal conductivity[19–23] (e.g., the nanostructuring and all-scale hierarchical architecturing). It is highly interesting to see if there are thermoelectric materials that operate in a desired temperature range and possess thermoelectric properties suitable for use under specific conditions.

Layered materials are interesting in that mixing different layers can improve thermoelectric properties[24–27] by increasing the power factor $S^2\sigma$ (via a change in the band gap and carrier density) and/or by reducing the lattice thermal conductivity κ_{lat} (via phonon scattering at the interfaces between different layers). The phases $(Bi_2Te_3)_m(PbTe)_n$[28–31] can be viewed as intergrowths of PbTe and Bi_2Te_3 phases,[32] and possess the structures similar to the tetradymite, Bi_2Te_2S, in which monoatomic layers of each element are stacked along the *c*-axis with rhombohedral symmetry ($R\bar{3}m$). The known homologues of $(Bi_2Te_3)_m(PbTe)_n$ include Bi_2Te_3 (m = 1, n = 0),[33] $PbBi_2Te_4$ (m = 1, n = 1),[34] and $PbBi_4Te_7$ (m = 2, n = 1).[35] Per unit cell, Bi_2Te_3 has three quintuple-layer (QL) slabs (Fig. 1a), $PbBi_2Te_4$ has three septuple-layer (SL) slabs (Fig. 1b), and $PbBi_4Te_7$ has alternating QL and SL slabs (Fig. 1c). In all three homologues adjacent slabs engage in Te. . .Te van der Waals interactions. The $(Bi_2Te_3)_m(PbTe)_n$ phases are good thermoelectric materials;[28–32,36–38] $PbBi_2Te_4$ (m = 1, n = 1) exhibits a very low thermal conductivity[29] and a high power factor $S^2\sigma = 14\times10^{-4}$ $W^{-1}K^{-2}$ at 600 K.[28,30] The ZT values of $PbBi_4Te_7$ (m = 2, n = 1) are as high as 0.5 even without optimizing the carrier concentration.[30,31] By analogy to the thermoelectric properties observed for mixed-layer compounds,[24–27] one might expect that $PbBi_4Te_7$ has enhanced thermoelectric properties than do Bi_2Te_3 and $PbBi_2Te_4$, since $PbBi_4Te_7$ consists of the slabs constituting Bi_2Te_3 and $PbBi_2Te_4$.

In the present work, we compare the electronic and thermoelectric properties of Bi_2Te_3, $PbBi_2Te_4$ and $PbBi_4Te_7$ on the basis of DFT calculations and thermoelectric transport property measurements. Contrary to our expectation, we found that $PbBi_4Te_7$ has the thermoelectric transport properties lying in between those of Bi_2Te_3 and $PbBi_2Te_4$, and the electronic structure of $PbBi_4Te_7$ around

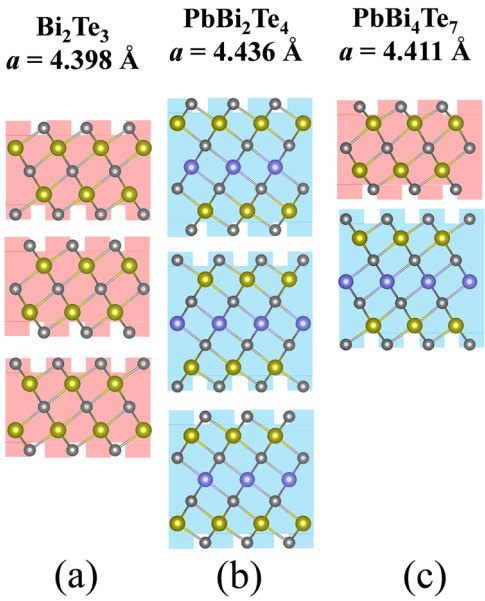

FIG. 1. Schematic projection views of the slabs in (a) Bi_2Te_3, (b) $PbBi_2Te_4$, and (c) $PbBi_4Te_7$ along the c-axis. Grey sphere = Te, gold sphere = Bi, and purple sphere = Pb.

the conduction and valence bands is very similar to those of Bi_2Te_3 and $PbBi_2Te_4$. This finding prompted us to consider a new class of mixed-slab thermoelectrics whose thermoelectric properties are approximated by the average of those of the constituent slabs. These thermoelectrics, to be termed "LEGO thermoelectrics", are important because their properties can be predicted once their constituent slab structures are known. In what follows we show that Bi_2Te_3, $PbBi_2Te_4$ and $PbBi_4Te_7$ are the first examples of LEGO thermoelectrics.

II. DETAILS OF CALCULATIONS

Our DFT calculations employed the frozen-core projector augmented wave method[39,40] encoded in the Vienna ab initio simulation package.[41] Unless specified otherwise, the generalized-gradient approximation of Perdew, Burke and Ernzerhof[42] was used for the exchange-correlation functional with the plane-wave-cut-off energy of 450 eV. The thermoelectric properties of Bi_2Te_3, $PbBi_2Te_4$, and $PbBi_4Te_7$ were calculated by using the BoltzTrap code,[43] which solves the semi-classical Boltzmann equation using the rigid band approach[44] under the constant relaxation time approximation. The electronic structures of Bi_2Te_3, $PbBi_2Te_4$, and $PbBi_4Te_7$ needed for these calculations were obtained by performing calculations with the Monkhorst-Pack k-points mesh of 30×30×10. The electrical conductivity σ was calculated under the assumption that the total electron momentum relaxation time τ is independent of energy. The latter approximation, though simple, has provided explanations for the thermoelectric properties of numerous systems.[45–49]

III. RESULTS AND DISCUSSION

A. Electronic structures

The total density of states (DOS) of Bi_2Te_3, $PbBi_2Te_4$, and $PbBi_4Te_7$ obtained from the calculations are presented in Fig. 2a. The lowest-occupied levels of the three compounds are taken to be identical in energy rather than their highest-occupied ones, so as to understand the origin of their band gap differences (see below). In addition, the highest-occupied energy level of $PbBi_2Te_4$ was

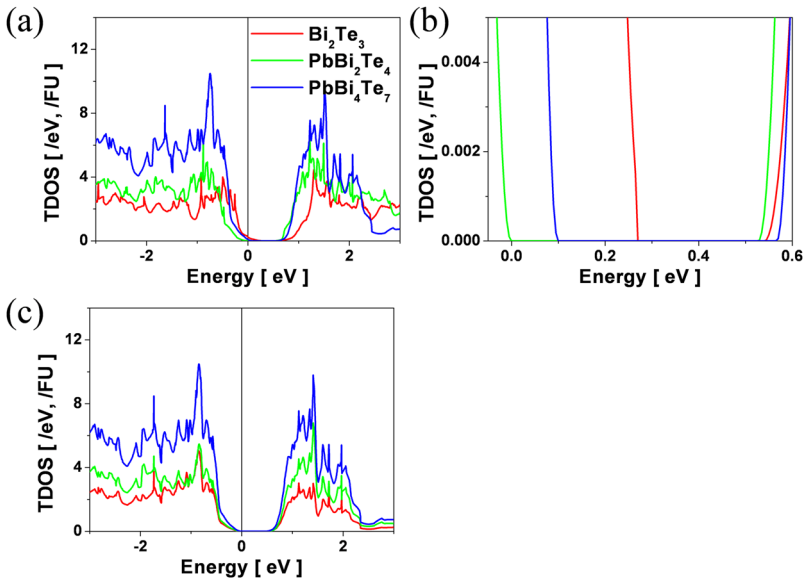

FIG. 2. (a) Total density of states (DOS) plots calculated for Bi_2Te_3, $PbBi_2Te_4$, and $PbBi_4Te_7$. (c) Zoomed-in view around the VBM and the CBM of Bi_2Te_3, $PbBi_2Te_4$, and $PbBi_4Te_7$. (b) Total DOS plot calculated for $PbBi_4Te_7$ and projected DOS plots calculated for the Bi_2Te_3 and $PbBi_2Te_4$ slabs of $PbBi_4Te_7$. In (a) and (b), the highest-occupied energy level of $PbBi_2Te_4$ was labeled as the energy zero. The red, green, and blue lines represent the total DOS plots calculated for Bi_2Te_3, $PbBi_2Te_4$, and $PbBi_4Te_7$, respectively.

labeled as the energy zero. A zoomed-in view around the valence band maximum (VBM) and the conduction band minimum (CBM) of Bi_2Te_3, $PbBi_2Te_4$, and $PbBi_4Te_7$ (Fig. 2b) shows that the three phases have nearly the same CBM but have the VBM increase in the order $PbBi_2Te_4$ < $PbBi_4Te_7$ < Bi_2Te_3. Consequently, the band gaps of the three phases increase in the order Bi_2Te_3 < $PbBi_4Te_7$ < $PbBi_2Te_4$. The calculated band gaps of $PbBi_2Te_4$, $PbBi_4Te_7$ and Bi_2Te_3 are 0.51, 0.37 and 0.27 eV, respectively. The results of our DFT calculations are in good agreement with those of the previous DFT studies.[32,50,51] The general feature of the total DOS of $PbBi_4Te_7$ (Fig. 2c) near the Fermi level is similar to the sum of the total DOS of Bi_2Te_3 and $PbBi_2Te_4$ (Fig. 2a,b), suggesting that the electronic structures of Bi_2Te_3 and $PbBi_2Te_4$ remain practically unmodified in the LEGO assembly $PbBi_4Te_7$. This indicates that the Te. . .Te interlayer van der Waals interactions in Bi_2Te_3, $PbBi_2Te_4$, and $PbBi_4Te_7$ are similar.

B. Thermoelectric properties

Within the rigid band approximation, the hole density can be introduced into a system by lowering the Fermi level E_F from the valence band maximum(VBM). If we define the chemical potential μ as

$$\mu = VBM - E_F \tag{2a}$$

then the hole density p is given by

$$p(\mu) = \frac{1}{V}\int_{\mu}^{0} N(E)dE \tag{2b}$$

where V is the unit cell volume. In a similar manner, the electron density can be introduced into a system by raising the Fermi level E_F from the conduction band minimum(CBM). If we define the chemical potential μ as

$$\mu = CBM - E_F \tag{3a}$$

then the electron density n is given by

$$n(\mu) = \frac{1}{V}\int_{0}^{\mu} N(E)dE. \tag{3b}$$

The p(E) vs. μ and n(E) *vs.* μ plots calculated for Bi_2Te_3, $PbBi_2Te_4$, and $PbBi_4Te_7$ are presented in Figs. 3a and 3b, respectively. The Seebeck coefficients S calculated for Bi_2Te_3, $PbBi_2Te_4$, and $PbBi_4Te_7$ as a function of μ reveal two extrema at $\mu = \pm 0.055$, ± 0.068, and ± 0.062 eV, respectively, with S values of ~ ± 440, ± 700, and ± 550 μV/K, respectively (Fig. 3c). The electrical conductivities of Bi_2Te_3, $PbBi_2Te_4$, and $PbBi_4Te_7$ normalized to the carrier lifetime τ, namely, σ/τ, as a function of chemical potential μ decrease in the order Bi_2Te_3 > $PbBi_4Te_7$ > $PbBi_2Te_4$ (Fig. 3d). Thus, the Seebeck coefficient S, the normalized electrical conductivity σ/τ, and the carrier life time τ of $PbBi_4Te_7$ lie in between those of Bi_2Te_3 and $PbBi_2Te_4$. The carrier life time plays an important role in governing the electron transport phenomena such as the electrical conductivity and the electron mobility in semiconductors.[52,53] Since the carrier life time of $PbBi_4Te_7$ lies in between those of Bi_2Te_3 and $PbBi_2Te_4$, the electrical properties of $PbBi_4Te_7$ are expected to lie in between those of Bi_2Te_3 and $PbBi_2Te_4$. This strongly supports that Bi_2Te_3, $PbBi_2Te_4$ and $PbBi_4Te_7$ form a group of LEGO thermoelectrics.

C. Experimental results and discussion

To verify experimentally that the Bi_2Te_3, $PbBi_2Te_4$ and $PbBi_4Te_7$ homologues are LEGO thermoelectrics, we carry out experiments. We prepared Bi_2Te_3 using the method described elsewhere.[54] To synthesize PBi_2Te_4 and $PbBi_4Te_7$, raw materials of Bi (99.999%, 5N Plus), Te (99.999%, 5N Plus) and Pb (99.995%, Aldrich) were melted in evacuated quartz ampoules by using conventional melting method. Mixtures of starting materials in evacuated silica tubes were melted at 1073 K for 5 h, annealed at 850 K for 96 h, and then quenched in water. The annealed ingots were pulverized by mortar and pestle, and then consolidated by using spark plasma sintering (Well Tech, WT 4000A) under an uniaxial pressure of 60 MPa at 753 K for 5 min.

Phase analysis of the sintered bodies was carried out by using an X-ray diffractometer (XRD, X'Pert-MPD, Philips). As shown in Fig. 4, the XRD pattern of each sample was in good agreement

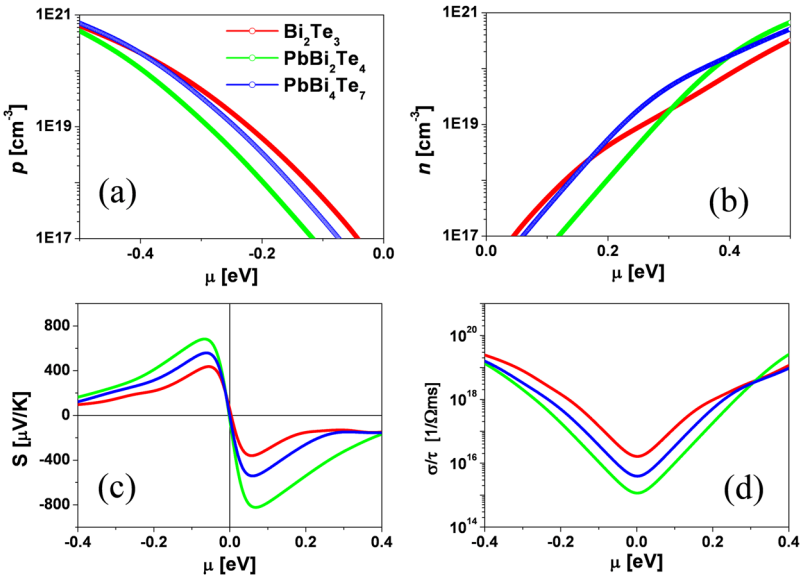

FIG. 3. Thermoelectric transport properties calculated for Bi_2Te_3, $PbBi_2Te_4$ and $PbBi_4Te_7$: (a) Hole density p vs. μ. (b) Electron density n vs. μ. (c) Seebeck coefficient S vs. μ. (d) Normalized electrical conductivity σ/τ vs. μ. The red, green, and blue curves refer Bi_2Te_3, $PbBi_2Te_4$, and $PbBi_4Te_7$, respectively.

with the standard powder pattern without any noticeable impurity peaks. Furthermore, the relative peak intensity in each pattern was similar to one another in all compounds, representing that the compounds had no significant preferential orientation.

Microstructural characterizations were performed by using a field emission scanning electron microscope (FESEM, JSM-6700F, JEOL). The grain size of each compound was similar to each other and was about a few tens of μm (Fig. 5). Furthermore, the grains were almost randomly distributed in all compounds, and it was consistent with the XRD results.

The temperature-dependent carrier concentrations and the Hall mobilities were determined by using a high-temperature Hall measurement system (HT-Hall, ResiTest 8300, Toyo). The Seebeck coefficient and the electrical conductivity were measured by a four probe method using a thermoelectric property measurement system (TPMS, RZ-2001i, Ozawa Science). All the transport

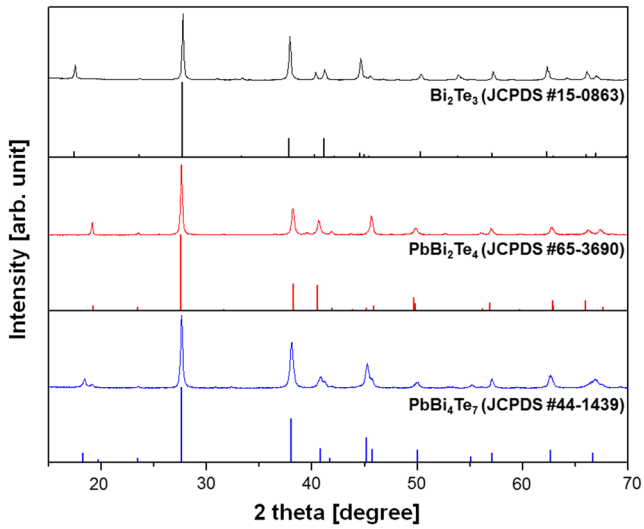

FIG. 4. XRD patterns of the sintered bodies of Bi_2Te_3, $PbBi_2Te_4$ and $PbBi_4Te_7$ compounds.

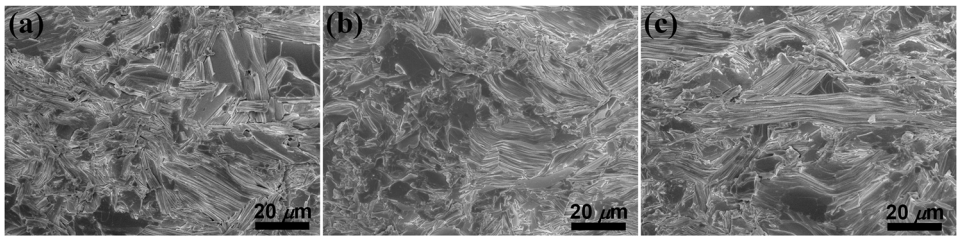

FIG. 5. SEM micrographs of the fractured surfaces of (a) Bi_2Te_3, (b) $PbBi_2Te_4$ and (c) $PbBi_4Te_7$.

properties were characterized along the direction perpendicular to the pressing axis of the SPS process.

The temperature-dependent carrier concentrations of Bi_2Te_3, $PbBi_2Te_4$ and $PbBi_4Te_7$ (Fig. 6a) show that they are almost independent of temperature. This indicates that these phases are degenerately doped by intrinsic point defects. Because the three phases were prepared by using a similar method without any intentional doping, the carrier concentration reflects the intrinsic ability for each building block to generate n-type carriers, which result most likely from Te-vacancies. The carrier concentrations in all compounds are almost independent of the temperature, indicating that all the compounds are highly degenerate semiconductors under this experimental condition.[36,54] On the other hand, their mobilities decrease with increasing the temperature due to the electron-phonon scattering.[36,54] It is noted that the charge transport properties of a semiconductor depend on the carrier lifetime τ.[55] By using the calculated σ/τ in Fig. 3d and experimental σ shown in the inset of Fig. 6a, the temperature-dependences of τ are calculated for Bi_2Te_3, $PbBi_2Te_4$, and $PbBi_4Te_7$ presented in Fig. 6b. This reveals that the carrier lifetime decreases in the order Bi_2Te_3 > $PbBi_4Te_7$ > $PbBi_2Te_4$. As shown in Fig. 6c, the mobility of Bi_2Te_3 is higher than those of $PbBi_2Te_4$ and $PbBi_4Te_7$, and the

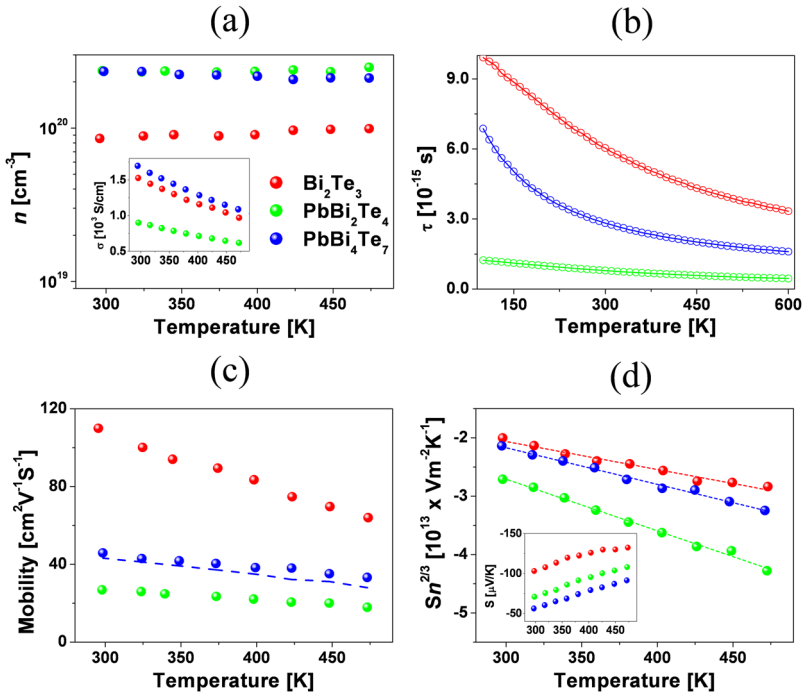

FIG. 6. Thermoelectric transport properties measured for Bi_2Te_3, $PbBi_2Te_4$ and $PbBi_4Te_7$: (a) Carrier concentration n as a function of temperature. The inset shows the temperature-dependence of the electrical conductivity σ. (b) Carrier life time τ calculated as a function of temperature. (c) Mobility as a function of temperature. (d) Plot of $Sn^{2/3}$ as a function of temperature. The red, green, and blue circles refer to the Bi_2Te_3, $PbBi_2Te_4$, and $PbBi_4Te_7$, respectively. The dashed line in (c) represents the harmonic average of the mobilities of Bi_2Te_3 and $PbBi_2Te_4$.

mobility of the mixed-slab phase $PbBi_4Te_7$ is very close to the harmonic average of the mobilities of Bi_2Te_3 and $PbBi_2Te_4$ as denoted by the blue dashed line. This result suggests strongly that the mobility in the mixed-slab phase is determined by the combined properties of each building block.[56] Furthermore, the layer-mixing effect can also be found in the effective mass, which can be estimated from the relationship,[57–59]

$$S = \frac{8\pi^2 k_B^2 T}{3eh^2} m^* \left(\frac{\pi}{3n}\right)^{2/3} \quad (4)$$

where k_B is the Boltzmann constant, e is the electron charge, h is the Plank constant, m^* is the effective mass, and n is the electron concentration. This relationship is derived for metals and degenerate semiconductors described by a parabolic band. Since we deal with the region of the CBM where the charge carriers are present, it is reasonable to use Eq. 4, which predicts a linear relationship for the $Sn^{2/3}$ vs. T plot. The latter is indeed the case for all three phases as shown in Fig. 6d. The effective masses estimated from the slopes of these plots are 0.76, 0.99, and 1.40 m_e for Bi_2Te_3, $PbBi_4Te_7$ and $PbBi_2Te_4$, respectively. Thus, the effective mass of $PbBi_4Te_7$ is quite close to the average of those of the Bi_2Te_3 and $PbBi_2Te_4$. Note that the linear $Sn^{2/3}$ vs. T plots found for Bi_2Te_3, $PbBi_4Te_7$ and $PbBi_2Te_4$ (Fig. 6d) are based on the S and n values obtained from the electronic band structure calculations presented in Fig. 3. This shows that Eq. 4, derived for metals and degenerate semiconductors described by a parabolic band, provides a very good description for the region of the CBM in Bi_2Te_3, $PbBi_4Te_7$ and $PbBi_2Te_4$.

IV. CONCLUDING REMARKS

From the electronic and thermoelectric properties examined for the three members of the layered phases $(Bi_2Te_3)_m(PbTe)_n$, i.e., (m, n) = (1, 0), (1, 1) and (2, 1), it is strongly suggested that they form a group of LEGO thermoelectrics whose thermoelectric properties can be approximated by the average of those of their constituent slabs. To further test the concept of LEGO thermoelectrics, it is desirable not only to prepare and characterize other members of $(Bi_2Te_3)_m(PbTe)_n$, but also to search for other groups of LEGO thermoelectrics.

ACKNOWLEDGMENTS

This research used resources of the National Energy Research Scientific Computing Center, DOE Office of Science User Facility supported by the Office of Science of the U.S. Department of Energy under Contract No. DE-AC02-05CH11231. It also was supported by the Nano Material Technology Development Program (2011-0030147), by the Midcareer Researcher Program (2018R1A2A2A05020902), and by Basic Science Research Program (NRF-2017R1D1A1B03036257) through the National Research Foundation of Korea (NRF), the Ministry of Education, Science and Technology, Republic of Korea.

[1] J. P. Heremans, Acta Physica Polonica **108**, 609 (2005).
[2] G. J. Snyder and E. S. Toberer, Nat. Mater. **7**, 105 (2008).
[3] G. J. Tan, L. D. Zhao, and M. G. Kanatzidis, Chem. Rev. **116**, 12123 (2016).
[4] D. M. Rowe, *CRC Handbook of Thermoelectrics* (CRC Press, Boca Raton, FL, 1995).
[5] G. Mahan, B. Sales, and J. Sharp, Physics Today **50**, 42 (1997).
[6] J. R. Sootsman, D.-Y. Chung, and M. G. Kanatzidis, Angew. Chem. Int. Ed. **48**, 8616 (2009).
[7] G. S. Nolas, J. Sharp, and H. J. Goldsmid, *Thermoelectrics: Basic principles and new materials developments* (Springer, Berlin, 2001).
[8] Y. Pei, A. D. LaLonde, and S. Iwanaga, Energy Environ. Sci. **4**, 2085 (2011).
[9] A. D. LaLonde, Y. Pei, and G. J. Snyder, Energy Environ. Sci. **4**, 2090 (2011).
[10] G. J. Snyder and E. S. Toberer, Nat. Mater. **7**, 105 (2008).
[11] L. D. Hicks, T. C. Harman, X. Sun, and M. S. Dresselhaus, Phys. Rev. B **53**, R10493 (1996).
[12] O. Delaire, J. MA, K. Marty, A. F. May, M. A. McGuire, M.-H. Du, D. J. Singh, A. Podlesnyak, G. Ehlers, M. D. Lumsden, and B. C. Sales, Nat. Mater. **10**, 614 (2011).
[13] R. Venkatasubramanian, E. Siivola, T. Colpitts, and B. O'Quinn, Nature **413**, 597 (20010).
[14] Y. Q. Cao, T. J. Zhu, X. B. Zhao, X. B. Zhang, and J. P. Tu, Appl. Phys. A **92**, 321 (2008).
[15] T. C. Harman, P. J. Taylor, M. P. Walsh, and B. E. LaForge, Science **297**, 2229 (2002).
[16] W. J. Xie, X. F. Tang, F. G. Yan, Q. J. Zhang, and T. M. Tritt, Appl. Phys. Lett. **94**, 102111 (2009).
[17] G. E. Lee, I. H. Kim, Y. S. Lim, W. S. Seo, B. J. Choi, and C. W. Hwang, J. Electron. Mater. **43**, 1650 (2014).
[18] K. C. Kim, S. H. Beak, H. J. Kim, D. B. Hyun, S. K. Kim, and J. S. Kim, J. Electron. Mater. **43**, 2000 (2014).

[19] Y. Lan, A. J. Minnich, G. Chen, and Z. F. Ren, Adv. Funct. Mater. **20**, 357 (2010).
[20] J. He, I. D. Blum, C.-I. Wu, T. P. Hogan, D. N. Seidman, V. P. Dravid, and M. G. Kanatzidis, Nature **489**, 414 (2012).
[21] X. Hu, P. Jood, M. Ohta, M. Kunii, K. Nagase, H. Nishiate, M. G. Kanatzidis, and A. Yamamoto, Energy Environ. Sci. **9**, 517 (2016).
[22] J. P. Heremans, V. Jovovic, E. S. Toberer, A. Saramat, K. Kurosaki, A. Charoenphakdee, S. Yamanaka, and G. J. Snyder, Science **321**, 554 (2008).
[23] C. J. Vineis, A. Shakouri, A. Majumdar, and M. G. Kanatzidis, Adv. Mater. **22**, 3970 (2010).
[24] C. Lee, J. Hong, M.-H. Whangbo, and J. H. Shim, Chem. Mater. **25**, 3745 (2013).
[25] C. Lee, J. Hong, W. R. Lee, D. Y. Kim, and J. H. Shim, J. Solid State Chem. **211**, 113 (2014).
[26] G. C. Tewari, T. S. Tripathi, and A. K. Rastogi, J. Electron. Mater. **39**, 1133 (2010).
[27] P. Jood and M. Ohta, **8**, 1124 (2015).
[28] L. A. Kuznetsova, V. L. Kuznetsov, and D. M. Rowe, J. Phys. Chem. Solids **61**, 1269 (2000).
[29] L. E. Shelimova, O. G. Karpinskii, P. P. Konstantinov, E. S. Avilov, M. A. Kretova, and V. S. Semskov, Inorg. Mater. **40**, 451 (2004).
[30] V. L. Kuznetsov, L. A. Kuznetsova, and D. M. Rowe, J. Phys. D: Appl. Phys. **34**, 700 (2001).
[31] T. Caillat, C. K. Huang, J.-P. Fleurial, G. J. Snyder, and A. Borshchevsky, Proceedings of the XVII International Conference on Thermoelectrics, Cardiff, UK, p151 (2000).
[32] L. Zhang and D. J. Singh, Phys. Rev. B **81**, 245119 (2010).
[33] V. V. Atuchin, T. A. Gavrilova, K. A. Kokh, N. V. Kuratieva, N. V. Pervukhina, and N. V. Surovtsev, Solid State Comm. **152**, 1119 (2012).
[34] R. Chami, G. Brun, J. C. Tedenac, and M. Maurin, Rev. Chim. Miner. **20**, 305 (1983).
[35] L. E. Shelimova, O. G. Karpinskii, T. E. Svechnikova, E. S. Avilov, and V. S. Zemskov, Inorg. Mater. **40**, 1264 (2004).
[36] J. Y. Tak, Y. S. Lim, J. N. Kim, C. Lee, J. H. Shim, H. K. Cho, C.-H. Park, and W.-S. Seo, J. Alloys. Comp. **690**, 966 (2017).
[37] T. V. Quang and M. Kim, J. Kor. Phys. Soc. **68**, 393 (2016).
[38] L. E. Shelimova, T. E. Svechnikova, P. P. Konstantinov, O. G. Karpinskii, E. S. Avilov, M. A. Kretova, and V. S. Zemskov, Inorg. Mater. **43**, 125 (2007).
[39] P. E. Blöchl, Phys. Rev. B **50**, 17953 (1994).
[40] G. Kresse and D. Joubert, Phys. Rev. B **59**, 1758 (1999).
[41] G. Kresse and J. Furthmüller, Phys. Rev. B **54**, 11169 (1996).
[42] J. P. Perdew, K. Burke, and M. Ernzerhof, 1996, **77**, 3865 (1966).
[43] G. K. H. Madsen and D. Singh, J. Comp. Phys. Commun. **175**, 67 (2006).
[44] T. Boker, R. Severin, A. Muller, C. Janowitz, R. Manzke, D. Vob, P. Kruger, A. Mazur, and J. Pollmann, Phys. Rev. B **64**, 235305 (2001).
[45] G. K. H. Madsen, K. Schwarz, P. Blaha, and D. J. Singh, Phys. Rev. B **68**, 125212 (2003).
[46] T. J. Scheidemantel, C. Ambrosch-Draxl, T. Thonhauser, J. V. Badding, and J. O. Sofo, Phys. Rev. B **68**, 125210 (2003).
[47] L. Lykke, B. B. Iversen, and G. K. H. Madsen, Phys. Rev. B **73**, 195121 (2006).
[48] H. G. Si, Y. X. Wang, Y. L. Yan, and G. B. Zhang, J. Phys. Chem. **116**, 3956 (2012), 12.
[49] C. Lee, T. An, E. E. Gordon, H. S. Ji, C. Park, J. H. Shim, Y. S. Lim, and M.-H. Whangbo, Chem. Mater. **29**, 2348 (2017).
[50] H. R. Aliabad and M. Kheirabadi, Physica B: Condens Mat. **433**, 157 (2014).
[51] S. V. Eremeev, G. Landolt, T. V. Menshchikova, B. Slomski, Y. M. Koroteev, Z. S. Aliev, M. B. Babanly, J. Henk, A. Ernst, L. Patthey, A. Eich, A. A. Khajetoorians, J. Hagemeister, O. Pietzsch, J. Wiebe, R. Wiesendanger, P. M. Echenique, S. S. Tsirkin, I. R. Amiraslanov, J. H. Dil, and E. V. Chulkov, Nat. Comm. **3**, 635 (2012).
[52] B. M. Askerov, *Electron Transport Phenomena in Semiconductors* (World Scientific, Singapore, 1994).
[53] N. W. Ashcroft and N. D. Mermin, *Solid State Physics* (Holt, Rinehart and Winston, New York, 1976).
[54] H. J. Yu, M. Jeong, Y. S. Lim, W.-S. Seo, O. Kwon, C.-H. Park, and H. Hwang, RSC Adv. **4**, 43811 (2014).
[55] J. N. Kim, M. Kaviany, and J. H. Shim, Phys. Rev. B **93**, 075119 (2016).
[56] Y. Takeda and T. P. Pearsall, Electron. Lett. **17**, 573 (1981).
[57] G. J. Snyder and E. S. Toberer, Nat. Mater. **7**, 105 (2008).
[58] J. Yang, H.-L. Yip, and A. K.-Y. Jen, Adv. Energy Mater. **3**, 549 (2013).
[59] Y. Xiao, G. Chen, H. Qin, M. Wu, Z. Xiao, J. Jiang, J. Xu, H. Jiang, and G. Xu, J. Mater. Chem. A **2**, 8512 (2014).